Microfluid Nanofluid
DOI 10.1007/s10404-014-1396-9

RESEARCH PAPER

Combining positive and negative magnetophoreses to separate particles of different magnetic properties

Taotao Zhu · Rui Cheng · Yufei Liu · Jian He · Leidong Mao

Received: 17 October 2013 / Accepted: 3 April 2014

Abstract A new separation method that combines both positive and negative magnetophoreses based on ferrofluids is used to separate mixtures of particles with different magnetic properties. Ferrofluids are stable magnetic nanoparticles suspensions. Under external magnetic field gradients, particles with a larger magnetization within the ferrofluids are attracted to a magnet while the ones with a smaller magnetization are pushed away from it. Based on this principle, we report the design, modeling, fabrication, and characterization of the separation device and use it to separate magnetic and non-magnetic particles, as well as particles with different magnetizations. This scheme is simple, cost-effective, and label-free compared to other existing techniques.

Keywords Separation · Ferrofluid · Microfluidics · Magnetophoresis

1 Introduction

Using magnetic beads for microfluidic cells manipulation, often referred to as "positive magnetophoresis," is an attractive alternative when compared to other competing techniques such as dielectrophoresis (Pamme 2006; Liu et al. 2009; Gijs et al. 2010; Nguyen 2012). Magnetic force is an "action at a distance;" it is not directly in contact with cells, minimizing potential hazardous effects that can reduce the viability of cells. The magnitude of this force is proportional to several parameters including volume of cells, difference in magnetizations between cells and their surrounding medium, and gradient of external magnetic fields (Rosensweig 1985; Jones 1995; Shevkoplyas et al. 2007). Representative applications of positive magnetophoresis in microfluidics include manipulation of paramagnetic beads or magnetically labeled cells under external fields. A typical example involves first labeling cells of interest with magnetic beads through either endocytosis or ligand–receptor interaction at their surfaces to render the cell beads conjugate magnetic. Because the magnetization of beads is usually larger than its surrounding medium (e.g., water), cell beads conjugates are magnetized under external fields and therefore move toward the location of field maximum. As a result, cells of interest can be separated from the rest of the sample and manipulated remotely. Positive magnetophoresis uses magnetic beads for labeling in order to achieve specific manipulation and separation. The process of incubating cells with magnetic beads can take up to several hours, and multiple washing steps are needed (Pamme and Wilhelm 2006; Robert et al. 2011), rendering the whole assay time-consuming and manually intensive. Furthermore, manipulation specificity of positive magnetophoresis depends on the magnetic moment of beads or loading of magnetic nanoparticles in cells. Magnetic moments of beads, even from the same batch, can vary dramatically due to their manufacturing procedure (van Ommering et al. 2006; Mihajlovic et al. 2007; Shevkoplyas et al. 2007; Tarn et al.

T. Zhu
Department of Chemistry, Nanoscale Science and Engineering Center, The University of Georgia, Athens, GA 30602, USA

R. Cheng · L. Mao (✉)
College of Engineering, Nanoscale Science and Engineering Center, The University of Georgia, Athens, GA 30602, USA
e-mail: mao@uga.edu

Y. Liu · J. He
Department of Physics and Astronomy, Clemson University, Clemson, SC 29634, USA

Published online: 23 April 2014

2009b). In addition, loading of magnetic nanoparticles in cells is greatly affected by their endocytotic capacities or ligand–receptor interactions and can vary among the same type of cells (Pamme and Wilhelm 2006; Jing et al. 2008; Robert et al. 2011). Therefore, it is highly beneficial to eliminate the labeling step associated with positive magnetophoresis and its application in cells manipulation.

A recent magnetic manipulative technique, termed as "negative magnetophoresis" (Jones 1995) is label-free and can address the above-mentioned problems (Kose et al. 2009; Krebs et al. 2009). The principle of negative magnetophoresis is exactly the opposite of positive magnetophoresis. In this case, magnetizations of cells are less than that of their surrounding medium, typically a magnetic fluid such as a paramagnetic salt solution (Peyman et al. 2009; Shen et al. 2012) or a ferrofluid (Kose et al. 2009; Zhu et al. 2010). Cells placed inside a magnetic fluid act as "magnetic holes" (Skjeltorp 1983). An externally applied magnetic field gradient attracts the fluid medium, which causes the cells to be preferentially pushed away (Rosensweig 1985). As such, cells and any other non-magnetic object inside these magnetic fluids can be potentially trapped, manipulated, and moved toward a weaker field direction without the time-consuming labeling step. The force acting on cells inside a magnetic fluid is named as magnetic buoyancy force, which is a body force and is proportional to the volume of cells (Rosensweig 1985). A typical application of negative magnetophoresis in size-based cells separation does not need any magnetic tags for labeling. Cells of different sizes were simply injected into a continuous-flow ferrofluid-filled microfluidic channel. Balanced by a diameter-dependent hydrodynamic viscous drag force, large cells experience more magnetic buoyancy force than smaller ones in ferrofluids, leading to a spatial separation between the two species at the end of the channel (Zhu et al. 2010, 2012).

Representative applications of negative magnetophoresis in microfluidics include cell and particle manipulation and separation in either a paramagnetic salt solution or a ferrofluid. The former generally has low susceptibility and magnetization. As a result, typical applications of a paramagnetic salt solution require either high fields from superconducting magnets (Tarn et al. 2009a; Vojtíšek et al. 2012) or high-field gradients from microfabricated ferromagnetic structures (Shen et al. 2012) to produce sufficient magnetic forces for manipulation. An ideal magnetic fluid that has relatively high susceptibility and magnetization under fields generated by permanent magnets is the ferrofluid. Ferrofluids are colloidal suspensions of magnetic nanoparticles, typically magnetite (Fe_3O_4) with diameters of approximately 10 nm (Rosensweig 1985). The nanoparticles are covered by either electrostatic or steric surfactants to keep them from aggregating and in suspension within a carrier medium. The susceptibility and magnetization of a ferrofluid are tunable through controlling its concentration of magnetic materials. For example, maximal volume fraction of a water-based magnetite ferrofluid is close to 10 %. Given the bulk magnetization of magnetite is 4.46×10^5 A/m, this ferrofluid's initial susceptibility is on the order of 1, and its saturation magnetization is on the order of 10^4 A/m under fields generated from a handheld permanent magnet, both of which are significantly larger than the values of a paramagnetic salt solution. Better magnetic properties of the ferrofluid enable its applications in a number of areas related to microfluidic manipulation. Examples include separation (Zhu et al. 2010, 2011b), deflection (Liang et al. 2011), focusing (Zhu et al. 2011a; Liang and Xuan 2012; Zeng et al. 2012), and assembly (Yellen et al. 2005; Erb et al. 2009; Krebs et al. 2009; Li and Yellen 2010; Khalil et al. 2012) of microparticles and cells. *Escherichia coli* and *Saccharomyces cerevisiae* (Baker's yeast) cells were separated from each other using a biocompatible ferrofluid with high throughput and efficiency in a continuous-flow fashion (Zhu et al. 2012). Sorting of particles and cells in ferrofluids was also demonstrated using traveling-wave magnetic fields generated from microfabricated electrodes (Kose et al. 2009; Kose and Koser 2012).

In most of the negative magnetophoresis-based microfluidic applications, the study of manipulation specificity is predominately focused on the difference in size or volume between objects (e.g., cells or particles) in magnetic fluids. The difference in magnetic properties (e.g., initial susceptibility or magnetization) between objects has not been investigated so far for the purpose of manipulation in ferrofluid-based negative magnetophoresis. On the other hand, although the manipulation specificity of positive magnetophoresis relies on the magnetic properties of beads, it typically can only distinguish magnetic objects from non-magnetic ones, lacking the ability of precise manipulation or separation based on their level of magnetization. This is not only because of the large variation of magnetic moments among beads or cells, but also due to the fact that traditional positive magnetophoresis takes place in water. In this study, by replacing water with ferrofluids of tunable magnetization, we add a new manipulation specificity to the traditional magnetophoresis. Beads or cells can now be manipulated based on their magnetization alone by adjusting the magnetization of their carrier liquid. This cannot be realized by using either positive or negative magnetophoresis individually. To this end, we will combine positive and negative magnetophoreses with the goal of separating particles of different magnetic properties in a microfluidic system coupled with a permanent magnet.

The remainder of this paper is organized as follows. First, we will demonstrate the working mechanism of

separating particles with different magnetic properties in ferrofluids and its feasibility through particle's trajectory simulation. We will then discuss experimental procedures including ferrofluids characterization and microfluidic experiments. "Results and discussion" part starts with a first demonstration on separating magnetic and non-magnetic particles in a custom-made ferrofluid, followed by a second demonstration on separating particles with different magnetic properties in a commercial ferrofluid. In the end, we will conclude our paper and provide an outlook of this technique in a potential application as a miniaturized magnetization measurement platform.

2 Working mechanism

A general expression of the magnetic force on a magnetized body in a magnetic fluid under a magnetic field is displayed as Eq. (1) (Rosensweig 1985). Here, $\mu_0 = 4\pi \times 10^{-7}$ H/m is the permeability of free space, V is the volume of the magnetized body, typically a superparamagnetic microparticle impregnated with magnetite nanoparticles, $\vec{M}_\mathrm{p}$ is its magnetization, $\vec{M}_\mathrm{f}$ is the magnetization of the magnetic fluid surrounding the body, and $\vec{H}$ is the magnetic field strength at the center of the body.

$$\vec{F} = \mu_0 V\left[\left(\vec{M}_\mathrm{p} - \vec{M}_\mathrm{f}\right)\cdot\nabla\right]\vec{H} \tag{1}$$

In a weak magnetic field on the order of 10^3 A/m, such as the one generated by microfabricated electrodes, magnetizations of both the body $\vec{M}_\mathrm{p}$ and the magnetic fluid $\vec{M}_\mathrm{f}$ depend approximately linearly on the applied field, resulting in $\vec{M}_\mathrm{p} = \chi_\mathrm{p}\vec{H}$ and $\vec{M}_\mathrm{f} = \chi_\mathrm{f}\vec{H}$, where χ_p and χ_f are the dimensionless initial magnetic susceptibilities of the body and the magnetic fluid, respectively. Therefore, magnetic force under weak field approximation takes the form as Eq. (2) that is often cited in the literature (Pamme 2006; Liu et al. 2009; Gijs et al. 2010), here $\vec{B}$ is magnetic flux density.

$$\vec{F} = \frac{V\left(\chi_p - \chi_f\right)}{\mu_0}\left(\vec{B}\cdot\nabla\right)\vec{B} \tag{2}$$

In a magnetic field generated by a handheld permanent magnet with its strength on the order of 10^6 A/m, Eq. (2) is no longer valid as the magnetization of a superparamagnetic particle depends nonlinearly on the applied field, so does the magnetization of a ferrofluid, both of which can be modeled accurately by the classical Langevin theory. Langevin theory considers magnetic nanoparticles in a superparamagnetic microparticle and a ferrofluid as a collection of monodispersed and non-interacting magnetic dipoles (Rosensweig 1985). This approach leads to the Langevin function of magnetization (Rosensweig 1985) in Eqs. (3) and (4). Here, $\alpha_\mathrm{p} = \mu_0\pi M_\mathrm{p,b} H d_\mathrm{p}^3 \big/ 6k_\mathrm{B}T$ and $\alpha_\mathrm{f} = \mu_0\pi M_\mathrm{f,b} H d_\mathrm{f}^3 / 6k_\mathrm{B}T$. ϕ_p and ϕ_f are volume fractions of the magnetic materials, $M_\mathrm{p,b}$ and $M_\mathrm{f,b}$ are saturation moments of the bulk magnetic materials, and d_p and d_f are the diameters of nanoparticles in a superparamagnetic microparticle and a ferrofluid, respectively. k_B is the Boltzmann constant, T is temperature. Equation (1) in conjunction with Langevin function of magnetization (Eqs. 3, 4) applies to more general cases than Eq. (2) alone. We will use Eqs. (1), (3), and (4) in subsequent simulations.

$$\frac{\vec{M}_\mathrm{p}}{\phi_\mathrm{p}\vec{M}_\mathrm{p,b}} = L(\alpha_\mathrm{p}) = \coth(\alpha_\mathrm{p}) - \frac{1}{\alpha_\mathrm{p}} \tag{3}$$

$$\frac{\vec{M}_\mathrm{f}}{\phi_\mathrm{f}\vec{M}_\mathrm{f,b}} = L(\alpha_\mathrm{f}) = \coth(\alpha_\mathrm{f}) - \frac{1}{\alpha_\mathrm{f}} \tag{4}$$

In the case of positive magnetophoresis, magnetization of the superparamagnetic particle $\vec{M}_\mathrm{p}$ is always larger than its surrounding fluid medium $\vec{M}_\mathrm{f}$. Under a non-uniform magnetic field, the direction of magnetic force $\vec{F}$ on the particle is pointing toward field maxima. On the other hand, for negative magnetophoresis, magnetization of the particle or cell $\vec{M}_\mathrm{p}$ is always less than its surrounding magnetic fluids $\vec{M}_\mathrm{f}$, and the direction of magnetic force $\vec{F}$ on the particle or cell is therefore pointing toward field minima. Both cases have been investigated extensively for their microfluidic applications, as they were reviewed in the "Introduction" section of this paper. However, few have considered the case where both positive and negative magnetophoreses coexist in one microfluidic system. In one of such cases, there exists two types of superparamagnetic particles with magnetizations of $\vec{M}_\mathrm{p1}$ and $\vec{M}_\mathrm{p2}$ in a magnetic fluid with magnetization of $\vec{M}_\mathrm{f}$. Firstly, $\vec{M}_\mathrm{p1}$ and $\vec{M}_\mathrm{p2}$ being both larger than $\vec{M}_\mathrm{f}$ will lead to a typical case of positive magnetophoresis while $\vec{M}_\mathrm{p1}$ and $\vec{M}_\mathrm{p2}$ being both less than $\vec{M}_\mathrm{f}$ will lead to negative magnetophoresis. In both cases, resulting magnetic forces depend not only on particles' magnetizations but also on their volumes. However, if $\vec{M}_\mathrm{f}$ is between $\vec{M}_\mathrm{p1}$ and $\vec{M}_\mathrm{p2}$, i.e., when the condition of $\vec{M}_\mathrm{p1} > \vec{M}_\mathrm{f} > \vec{M}_\mathrm{p2}$ is met, magnetic force will attract particles Type 1 toward field maxima while pushes particles Type 2 away toward field minima, as shown in Fig. 1a. It should be noted here that the volume of particles now only affects the magnitude, but not the direction of magnetic forces. This way, particles can be distinguished and sorted solely based on their magnetizations in a simple microfluidic channel with a permanent magnet, as illustrated in Fig. 1b. The dynamics of particles in the microchannel is determined primarily by the balance of the magnetic force

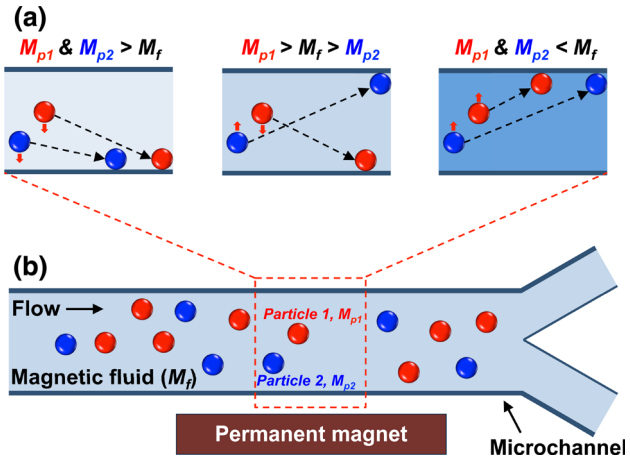

Fig. 1 Schematic representation of combining positive and negative magnetophoreses in a ferrofluid to separate particles of different magnetic properties. **a** Particles with different magnetic properties experience either positive or negative magnetophoresis and hence have different trajectories in a microfluidic device (**b**). *Left illustration* of **a** is the case where both types of particles experience positive magnetophoresis, *right illustration* of **a** is where both types of particles experience negative magnetophoresis. In *middle illustration* of **a**, both positive and negative magnetophoreses exist

and the hydrodynamic viscous drag force (Zhu et al. 2011b). The magnetic force scales with the volume of a particle, while the hydrodynamic drag force scales with the diameter of a particle. Therefore, the velocity of a particle moving toward or away from a magnetic field gradient depends on the square of the diameter.

3 Materials and methods

Two types of ferrofluids are used in the microfluidic experiments. One of them is a water-based magnetite nanoparticle ferrofluid stabilized by sodium oleate surfactant. The nanoparticles are prepared through a chemical co-precipitation process (Massart 1981), which involves adding a mixture of iron(II) chloride tetrahydrate and iron(III) chloride hexahydrate into an ammonium hydroxide solution. The gelatinous precipitate is washed, followed by the addition of sodium oleate solution and sonication. A second ferrofluid is a commercial water-based magnetite nanoparticle ferrofluid (EMG 408, Ferrotec Co., Bedford, NH) stabilized by proprietary anionic surfactants. Magnetization curves of both ferrofluids are measured using a vibrating sample magnetometer (VSM). Two fluorescent polystyrene non-magnetic particles (green 4.2 μm diameter, Thermo Fisher Scientific Inc., Waltham, MA, and green 7.3 μm diameter, Bangs Laboratories Inc., Fishers, IN), and four fluorescent superparamagnetic particles (red 2.6 μm diameter, green 2.8 μm diameter, green 7.9 μm diameter, green 8.2 μm diameter, Bangs Laboratories Inc., Fishers, IN) are used in the experiments.

We measure the field-dependent direct current (DC) magnetizations of our ferrofluid samples using a VSM on a physical property measurement system (PPMS) (Model P525, Quantum Design Inc., San Diego, CA). The ferrofluid sample is injected into a plastic cylindrical capsule using a syringe, sealed by a small amount of super glue, and then tested for sealing in vacuum. Sample mass is determined by differentiating the mass before and after filling the capsule. The mass is chosen to be between 10 and 15 mg to ensure both the intensity of magnetic signals and a small vertical sample size. Total mass of the ferrofluid sample and super glue is also checked before and after the sealing test. Magnetic signals of the empty capsule and super glue are confirmed to be negligible. Typically, two to three samples of the same nominal composition are prepared and measured to check the reproducibility of measurements. The measurements are taken at 300 K and at a vibrating frequency of 40 Hz. The applied field sweeps between ±3,183 kA/m at a rate of 3,183 A/m per second.

The prototype polydimethylsiloxane (PDMS) microfluidic device is fabricated through a standard soft-lithography approach (Xia and Whitesides 1998) and attached to a flat surface of another piece of PDMS, as shown in Fig. 2a, b. A mask of the device pattern is designed using AutoCAD 2008 (Autodesk Inc., San Rafael, CA) and printed by a commercial photo-plotting company (CAD/Art Services Inc, Bandon, OR). Dimensions of the microfluidic channel are listed in Fig. 2c, d. Thickness of the device is measured to be 38 μm by a profilometer (Dektak 150, Veeco Instruments Inc., Chadds Ford, PA). Before attachment, channel surface is treated with air plasma (PDC-32G plasma cleaner, Harrick Plasma, Ithaca, NY) at 11.2 Pa O_2 partial pressure with 18 W power for 1 min. One neodymium–iron–boron (NdFeB) permanent magnet is embedded into the microchannel with its magnetization direction pointing along the y axis as indicated in Fig. 2a, c during PDMS curing stage. The magnet is 25.4 mm in length, 3.175 mm in width, and 3.175 mm in thickness. The magnet is placed 2 mm away from the edge of the channel. Magnetic flux density at the center of the magnetic surface is measured to be 470 mT by a Gauss meter (Model 5080, Sypris, Orlando, FL) and an axial probe with 0.381 mm diameter of circular active area. Before experiments, the device is treated again with air plasma for 10 min and then washed with 1 % Triton-X solution to render the microchannel surfaces hydrophilic and reduce particles' attachment.

Microfluidic experiments are conducted on the stage of an inverted microscope (Zeiss Axio Observer, Carl Zeiss Inc., Germany). A mixture of ferrofluids and particles is injected into a microchannel and maintained at a tunable flow rate using a syringe pump (Nexus 3000, Chemyx Inc.,

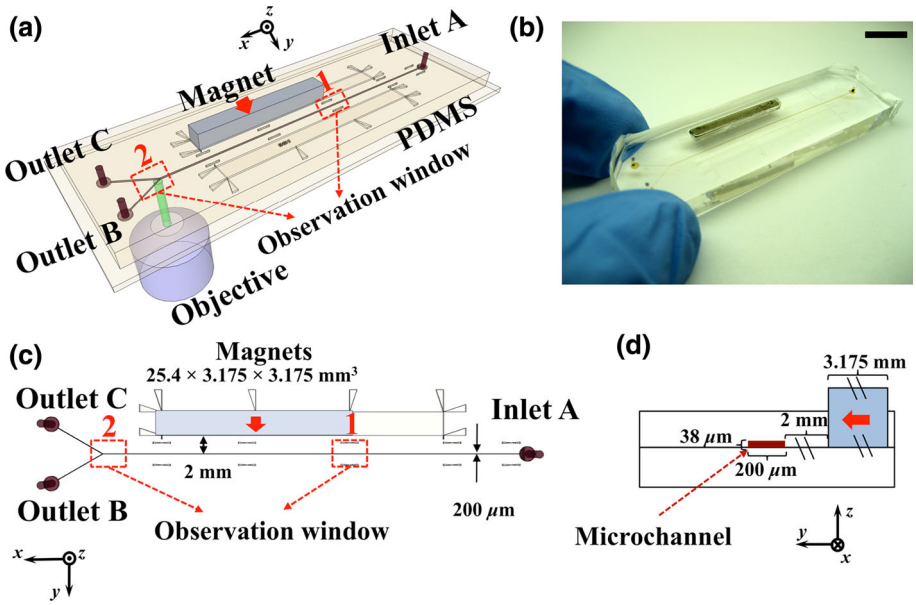

Fig. 2 Device illustrations. **a** Schematic drawing of the microfluidic device with a permanent magnet and a microchannel. **b** An image of prototype device. *Scale bar* is 10 mm. **c** *Top view* of the device and relevant dimensions. *Red arrows* indicate the direction of magnets' magnetization. **d** *Cross section* of the device. The origin of the device and the simulation plots in Fig. 3 are located at the center of the microchannel in all three dimensions (color figure online)

Stafford, TX). Micrographs of particles are recorded using bright-field mode and fluorescent mode through either a green fluorescent filter set (41001 FITC, Chroma Technology Corp., Rockingham, VT) or a red filter set (43HE, Carl Zeiss Inc., Germany), and a CCD camera (SPOT RT3, Diagnostic Instruments, Inc., Sterling Heights, MI).

In this paper, we extend our two-dimensional analytical model of particles' transport in ferrofluids (Zhu et al. 2011b) to three dimensions in order to enable fast and accurate predications for trajectories of microparticles with different magnetizations in a microfluidic system. We choose to use an analytical approach over numerical ones because of its advantages in simulation speed and accuracy (Zhu et al. 2011b). We obtain three-dimensional particles' trajectories in microchannels by first calculating magnetic buoyancy force (Eq. 1) on particles using a three-dimensional analytical model of magnetic field distribution and a nonlinear magnetization model of ferrofluids (Eqs. 3, 4) inside the microchannel, then deriving and solving governing equations of motion for particles in laminar flow conditions using analytical expressions of magnetic buoyancy and hydrodynamic drag forces.

4 Results and discussion

We start with simulation results in Fig. 3 that depict distributions of magnetic fields and magnetic forces on a 4-μm-diameter particle within the microchannel, as well as the representative trajectories of that particle with different magnetizations in a ferrofluid in all three dimensions. Figure 3a shows a surface plot of the magnitude of magnetic fields in the x–y plane at $z = 0$ within the channel. Magnetic fields decay quickly and form a gradient pointing toward the negative y direction. The gradient leads to a magnetic buoyancy force on the non-magnetic particle ($\phi_p = 0$) pointing toward the positive y direction, as shown in Fig. 3b. Figure 3c shows the relationship between the particle's trajectory and its magnetic volume fractions. Here, we fix the magnetic volume fraction of the ferrofluid at 1 %, very close to the measured value of the EMG 408 commercial ferrofluid that will be used in later experiments. Based on the analysis before, a particle having a smaller magnetic volume fraction (<1 %) than the surrounding fluid experiences negative magnetophoresis and is pushed away from the magnet, while a particle with a larger magnetic volume fraction (>1 %) experiences positive magnetophoresis and is attracted toward the magnet. When the magnetic volume fractions of both the particle and the fluid match exactly ($\phi_p = \phi_f = 1$ %), the particle experiences so-called isomagnetophoresis(Kang et al. 2008; Hahn and Park 2011) and retains its laminar flow path without deflection. Figure 3d–f illustrates the distributions of magnetic field and force, as well as trajectories of the particle in the y–z plane at $x = 0$; Fig. 3g–i illustrates the case for x–z plane at $y = 0$.

In order for positive and negative magnetophoreses to coexist, the ferrofluid's magnetization $\vec{M}_f$ needs to be between the particles' magnetizations$\vec{M}_{p1}$ and $\vec{M}_{p2}$. Magnetic force will then attract one type of particle while repel the other and result in spatial separation of the two. It is therefore critical to determine the magnetization of ferrofluid and both particles at a specific magnetic field, most relevant to actual experimental conditions. Saturation magnetization of both 2.6 and 2.8 μm particles (categorized as ~3 μm particles) is 10,019 A/m, while saturation

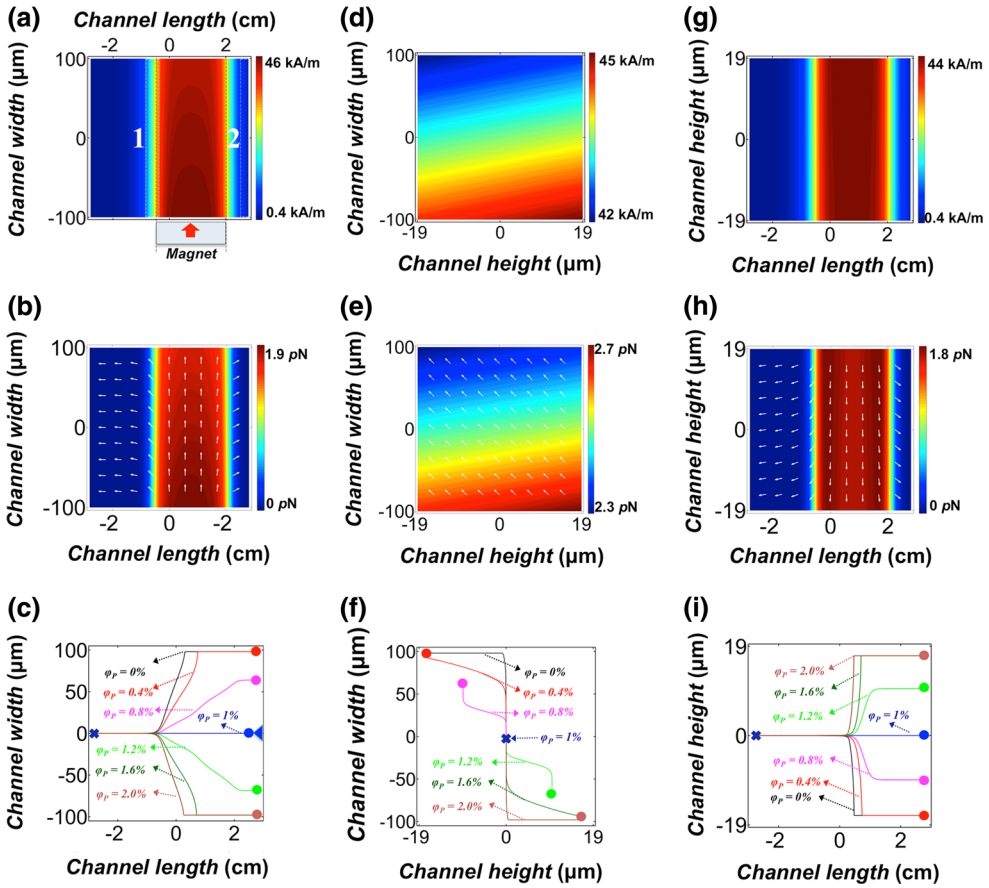

Fig. 3 Analytical three-dimensional simulation of magnetic field and force distributions in microfluidic channel, and trajectories of 4-μm-diameter particles with different magnetic volume fractions. **a**–**c** *x*–*y* plane ($z = 0$), **d**–**f** *y*–*z* plane ($x = 0$), **g**–**i** *x*–*z* plane ($y = 0$) of magnetic field strength (surface plot) (**a**, **d**, **g**), magnetic force (*surface plot* force magnitude; *arrow plot* force direction, both are calculated on a 4-μm-diameter non-magnetic particle) (**b**, **e**, **h**), and particles' trajectories (**c**, **f**, **i**). Magnetic volume fraction of the ferrofluid is chosen to be 1 %, while particles have 0, 0.4, 0.8, 1, 1.2, 1.6, and 2 % of magnetic volume fractions. Ferrofluid flow rate is 1.5 μl/min. Other simulation parameters match exact experimental conditions. *Crosses* indicate starting points, while *solid circles* indicate ending points of particles' trajectories. *Blue triangle* in **c** indicates boundary between outlets. The starting points are chosen to be at the center of the channel to allow both positive and negative deflections in *y* direction for different ferrofluid volume fractions (color figure online)

magnetization of 7.9 and 8.2 μm particles (categorized as ~8 μm particles) is approximately 2,939 A/m. It should be noted that the magnetization is measured on a specific batch of sample containing many particles, then averaged per unit volume. It is an average property of a large number of particles, actual magnetization of individual particle may vary significantly within the same batch (van Ommering et al. 2006), and magnetization of one batch may vary from another. We only use the magnetization curve as a rough estimate for particles' magnetization in the following separation experiments. The saturation magnetization of the ferrofluid is measured to be 571 A/m, corresponding to a 0.1 % magnetic material content within the ferrofluid, given the saturation magnetization of bulk magnetite is 4.46×10^5 A/m. The saturation magnetization of the EMG 408 commercial ferrofluid is measured to be 4,953 A/m, corresponding to a 1.1 % magnetic material content.

The average magnetic field strength within the microchannel is estimated to be on the order of 10 kA/m, as shown in Fig. 3. Under this field, the magnetization of the ferrofluid stabilized by sodium oleate falls between that of non-magnetic particles and magnetic particles, which enables us to separate them in this ferrofluid as a first demonstration of combining positive and negative magnetophoreses. Our goal is to demonstrate the separation of particles based on their magnetic properties instead of their sizes. Therefore, we choose two groups of particles with similar sizes. Magnetic particles are selected to have higher saturation magnetization than that of the sodium oleate ferrofluid, while non-magnetic particles have smaller saturation magnetization. Furthermore, the magnetization of the commercial EMG 408 ferrofluid falls between that of the magnetic particle with ~8 μm diameter and the magnetic particle with ~3 μm diameter. We will use them as a second demonstration to separate particles with different magnetic properties.

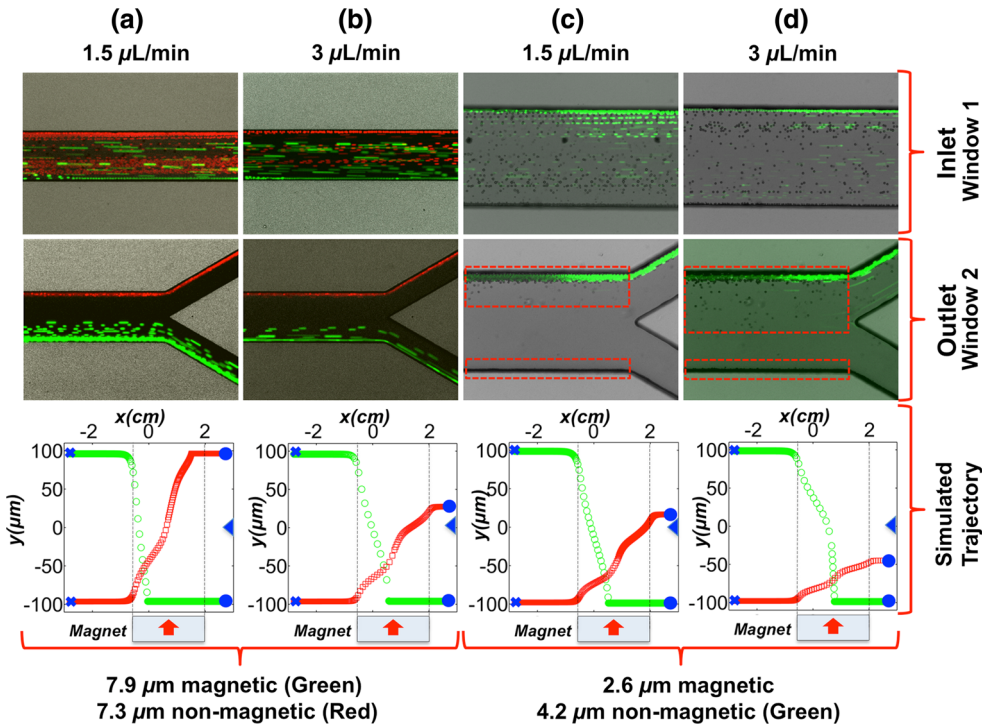

Fig. 4 Experimental composite micrographs of the separation process between non-magnetic and magnetic particles and simulated particles' trajectories. *a* and *b* are mixture of 7.3 μm non-magnetic and 7.9 μm magnetic at flow rates of 1.5 and 3 μl/min, respectively. *c* and *d* are mixture of 4.2 μm non-magnetic and 2.6 μm magnetic at flow rates of 1.5 and 3 μl/min, respectively. *Top image* is at observation window 1, *middle image* is at observation window 2, and *bottom plot* is simulated trajectory of the particles when magnetic field is present. *Crosses* indicate starting points, while *solid circles* indicate ending points of simulated particles' trajectories. The starting points are chosen at extreme opposite locations of the channel to capture realistic experimental conditions. *Blue triangle* in simulated trajectory plots indicates the boundary between outlets. Channel width is 200 μm (color figure online)

We first demonstrate the separation of 7.3 μm non-magnetic particles (red fluorescent) and 7.9 μm magnetic particles (green fluorescent) in the ferrofluid stabilized by sodium oleate, as shown in Fig. 4a, b. We introduce a ferrofluid/particle mixture into the microfluidic channel inlet A at a constant flow rate of 1.5 μl/min. An observation window is located at before the left edge of the magnet (window 1), and another at the outlets (window 2), as indicated in Fig. 2c. The top image of Fig. 4a records particles' trajectories close to the inlet at window 1. Prior to window 1, the magnetic field and its gradient are present but significantly smaller than those of the area right below the magnet, resulting in a smaller magnitude of magnetic buoyancy forces in *y* direction (vertical to the flow direction) on both non-magnetic and magnetic particles. Both particles are thus observed in fluorescent mode flowing together across the channel width. On the other hand, middle image of Fig. 4a records particles' trajectories close to the outlets at window 2. Between windows 1 and 2, both particles experience significant magnetic buoyancy force on them because of the larger magnetic field and its gradient in *y* direction. The force on non-magnetic particles is pointing in positive *y* direction (weaker field direction) due to negative magnetophoresis, while the force on magnetic particles is pointing in negative *y* direction (stronger field direction) due to positive magnetophoresis. This leads to the spatial separation of two types of particles at the outlets, which is also confirmed by the simulation result in the bottom plot of Fig. 4a. Similar separation phenomenon still exists at an increased flow rate of 3 μl/min, as shown in Fig. 4b.

We then demonstrate the separation of 4.2 μm non-magnetic particles (green fluorescent) and 2.6 μm magnetic particles in the same ferrofluid. About 2.6 μm magnetic particles are fluorescently red. However, since their fluorescence alone is weak and difficult to observe in our microscope setup, we instead choose to use a combination of both bright-field and fluorescent modes microscopy to record the separation process. Figure 4c, d records the process at windows 1 and 2 with flow rates of 1.5 and 3 μl/min. In both cases, magnetic particles are separated from non-magnetic particles. However, at the increased flow rate of 3 μl/min, the width of the non-magnetic particle stream expands and some of the non-magnetic particles exit the channel through the bottom outlet, which is predicted by the 3D simulation in the bottom plot of Fig. 4d. Generally

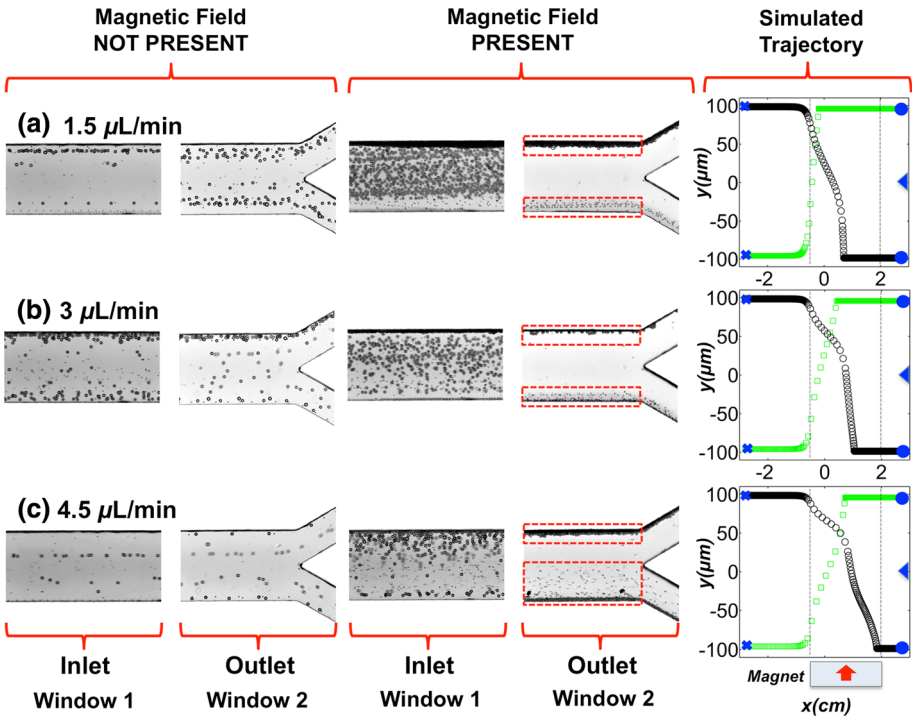

Fig. 5 Experimental composite micrographs of the separation process between particles with different magnetic properties and simulated particles' trajectories. Mixture of 2.8 μm strongly magnetic and 8.2 μm weakly magnetic particles is recorded at flow rates of *a* 1.5 μl/min, *b* 3 μl/min, and *c* 4.5 μl/min, respectively. *Left images* are at observation windows 1 and 2 when magnetic field is not present, *middle images* are at observation windows 1 and 2 when magnetic field is present, and *right plot* is simulated trajectory of the particles when magnetic field is present. *Green squares* represent 8.2 μm weakly magnetic particles, while *black circles* represent 2.8 μm strongly magnetic particles. *Crosses* indicate starting points, while *solid circles* indicate ending points of simulated particles' trajectories. The starting points are chosen at extreme opposite locations of the channel to capture realistic experimental conditions. *Blue triangle* in simulated trajectory plots indicates the boundary between outlets. Channel width is 200 μm (color figure online)

speaking, the particle deflection has a strong dependence on the magnitude of ferrofluid flow rates. When the flow rate increases, the residual time of the particles in the microchannel decreases, resulting in a smaller deflection for the particle, provided that all other experimental parameters are constant. This is confirmed in both simulation and experimental results in Fig. 4.

We move onto the demonstration of separating of 8.2 μm magnetic particles (saturation magnetization ~2,939 A/m) and 2.8 μm magnetic particles (saturation magnetization ~10,019 A/m) in the EMG 408 ferrofluid (saturation magnetization 4,953 A/m), as shown in Fig. 5. Again, we emphasize that the magnetization values of particles are provided by the manufacturer and are measured on a specific batch of sample. Actual magnetization of the sample used in this experiment may vary from these values. A more precise way to obtain magnetization curves of these particles is to measure them using VSM. However, because of the cost of the sample, we choose to use the manufacturer data and leave the VSM measurement to the time when precise magnetization curves are needed. The EMG 408 commercial ferrofluid has a saturation magnetization of 4,953 A/m that falls roughly halfway between the ones of 8.2 and 2.8 μm magnetic particles, making it ideal to separate them.

We introduce ferrofluids/particles mixture into the microfluidic channel inlet A at constant flow rates of 1.5, 3, and 4.5 μl/min. The trajectories of particles are recorded and compared at windows 1 and 2 between the cases when a magnetic field is and is not present. Figure 5a shows the comparison at a 1.5 μl/min flow rate. When the magnetic field is not present, magnetic particles flow together in the microchannel and exit the channel through both outlets as expected. As soon as the magnetic field is present, a clear migration of 2.8 μm particles toward the stronger field direction and 8.2 μm particles toward the weaker field direction is observed. Streams of both particles are labeled with red dashed boxes on Fig. 5a. The migration of particles toward different directions is the evidence that both positive and negative magnetophoreses exist in this system, as confirmed by the simulation particle trajectory using our 3D model. We exploit it to separate magnetic particles solely based on their magnetic properties, regardless of their sizes. Figure 5b shows the comparison case at a 3 μl/

min flow rate where similar separation process is observed. Increasing the flow rate further to 4.5 μl/min results in shorter residual time of particles in the channel, which leads to the expansion of the width of 2.8 μm particles, as shown in Fig. 5c.

5 Conclusions

In summary, we developed a new separation method based on particles' magnetic properties through combining positive and negative magnetophoreses in a ferrofluid. The principle of this method is to use a ferrofluid with its magnetization between that of the particles, which leads to particles with larger magnetization being attracted and the ones with smaller magnetization being pushed away from the maxima of magnetic fields. Using this method, we demonstrate the separation of magnetic and non-magnetic particles in a custom-made ferrofluid. We also demonstrate the separation of particles with different magnetic properties in a commercial ferrofluid. We stated in the "Introduction" section that positive magnetophoresis needed labeling steps while negative magnetophoresis could be label-free. It should be noted here that the technique of combining both positive and negative magnetophoreses inevitably needed labeling steps for the objects to be manipulated. The advantage of being label-free from negative magnetophoresis is forfeited for the goal of distinguishing particles or cells that have various degrees of magnetization.

We picture this method can be used to separate particles with smaller difference in their magnetic properties than the case demonstrated in this paper using ferrofluids of tunable concentrations. A potential application as well as a future work of this method is to apply it as a miniaturized measurement platform for characterizing magnetizations of microparticles or cells. In such a platform, particles or cells with different magnetizations will be introduced into a microchannel where a linear gradient of ferrofluids is created across the channel width. Under a non-uniform magnetic field, they will keep migrating across the channel width because of the magnetic buoyancy force until their magnetization equals the surrounding ferrofluid and the resulting magnetic buoyancy force vanishes. As a result, the steady-state position of the particles and cells reveals their magnetization under a specific magnetic field. By varying the field strength, a series of magnetization values can be obtained and used to construct a magnetization curve for these particles or cells. We envision such a platform providing a low-cost, simplified, and fast (measurement time is on the order of seconds) alternative to traditional macroscale magnetization measurement systems.

Acknowledgments Research reported in this publication was supported by the National Institute of General Medical Sciences of the National Institutes of Health under Award Number R21GM104528. The content is solely the responsibility of the authors and does not necessarily represent the official views of the National Institutes of Health.

References

Erb RM, Son HS, Samanta B, Rotello VM, Yellen BB (2009) Magnetic assembly of colloidal superstructures with multipole symmetry. Nature 457(7232):999–1002. doi:10.1038/Nature07766

Gijs MAM, Lacharme F, Lehmann U (2010) Microfluidic applications of magnetic particles for biological analysis and catalysis. Chem Rev 110(3):1518–1563. doi:10.1021/Cr9001929

Hahn YK, Park JK (2011) Versatile immunoassays based on isomagnetophoresis. Lab Chip 11(12):2045–2048. doi:10.1039/C0lc00569j

Jing Y, Mal N, Williams PS, Mayorga M, Penn MS, Chalmers JJ, Zborowski M (2008) Quantitative intracellular magnetic nanoparticle uptake measured by live cell magnetophoresis. Faseb J 22(12):4239–4247. doi:10.1096/Fj.07-105544

Jones TB (1995) Electromechanics of particles. Cambridge University Press, Cambridge

Kang JH, Choi S, Lee W, Park JK (2008) Isomagnetophoresis to discriminate subtle difference in magnetic susceptibility. J Am Chem Soc 130(2):396–397. doi:10.1021/Ja0770678

Khalil KS, Sagastegui A, Li Y, Tahir MA, Socolar JES, Wiley BJ, Yellen BB (2012) Binary colloidal structures assembled through Ising interactions. Nat Commun 3:794. doi:10.1038/Ncomms1798

Kose AR, Koser H (2012) Ferrofluid mediated nanocytometry. Lab Chip 12(1):190–196. doi:10.1039/C1lc20864k

Kose AR, Fischer B, Mao L, Koser H (2009) Label-free cellular manipulation and sorting via biocompatible ferrofluids. Proc Natl Acad Sci USA 106(51):21478–21483. doi:10.1073/Pnas.0912138106

Krebs MD, Erb RM, Yellen BB, Samanta B, Bajaj A, Rotello VM, Alsberg E (2009) Formation of ordered cellular structures in suspension via label-free negative magnetophoresis. Nano Lett 9(5):1812–1817. doi:10.1021/Nl803757u

Li KH, Yellen BB (2010) Magnetically tunable self-assembly of colloidal rings. Appl Phys Lett 97(8):083105. doi:10.1063/1.3483137

Liang LT, Xuan XC (2012) Diamagnetic particle focusing using ferromicrofluidics with a single magnet. Microfluid Nanofluidics 13(4):637–643. doi:10.1007/S10404-012-1003-X

Liang LT, Zhu JJ, Xuan XC (2011) Three-dimensional diamagnetic particle deflection in ferrofluid microchannel flows. Biomicrofluidics 5(3):034110. doi:10.1063/1.3618737

Liu CX, Stakenborg T, Peeters S, Lagae L (2009) Cell manipulation with magnetic particles toward microfluidic cytometry. J Appl Phys 105(10):102014. doi:10.1063/1.3116091

Massart R (1981) Preparation of aqueous magnetic liquids in alkaline and acidic media. IEEE Trans Magn 17(2):1247–1248. doi:10.1109/Tmag.1981.1061188

Mihajlovic G, Aledealat K, Xiong P, Von Molnar S, Field M, Sullivan GJ (2007) Magnetic characterization of a single superparamagnetic bead by phase-sensitive micro-Hall magnetometry. Appl Phys Lett 91(17):172518. doi:10.1063/1.2802732

Nguyen N-T (2012) Micro-magnetofluidics: interactions between magnetism and fluid flow on the microscale. Microfluid Nanofluidics 12(1–4):1–16. doi:10.1007/s10404-011-0903-5

Pamme N (2006) Magnetism and microfluidics. Lab Chip 6(1):24–38. doi:10.1039/B513005k

Pamme N, Wilhelm C (2006) Continuous sorting of magnetic cells via on-chip free-flow magnetophoresis. Lab Chip 6(8):974–980. doi:10.1039/B604542a

Peyman SA, Kwan EY, Margarson O, Iles A, Pamme N (2009) Diamagnetic repulsion—a versatile tool for label-free particle handling in microfluidic devices. J Chromatogr A 1216(52):9055–9062. doi:10.1016/j.chroma.2009.06.039

Robert D, Pamme N, Conjeaud H, Gazeau F, Iles A, Wilhelm C (2011) Cell sorting by endocytotic capacity in a microfluidic magnetophoresis device. Lab Chip 11(11):1902–1910. doi:10.1039/C0lc00656d

Rosensweig RE (1985) Ferrohydrodynamics. Cambridge University Press, Cambridge

Shen F, Hwang H, Hahn YK, Park JK (2012) Label-free cell separation using a tunable magnetophoretic repulsion force. Anal Chem 84(7):3075–3081. doi:10.1021/Ac201505j

Shevkoplyas SS, Siegel AC, Westervelt RM, Prentiss MG, Whitesides GM (2007) The force acting on a superparamagnetic bead due to an applied magnetic field. Lab Chip 7(10):1294–1302. doi:10.1039/B705045c

Skjeltorp AT (1983) One-dimensional and two-dimensional crystallization of magnetic holes. Phys Rev Lett 51(25):2306–2309. doi:10.1103/Physrevlett.51.2306

Tarn MD, Hirota N, Iles A, Pamme N (2009a) On-chip diamagnetic repulsion in continuous flow. Sci Technol Adv Mater 10(1):014611. doi:10.1088/1468-6996/10/1/014611

Tarn MD, Peyman SA, Robert D, Iles A, Wilhelm C, Pamme N (2009b) The importance of particle type selection and temperature control for on-chip free-flow magnetophoresis. J Magn Magn Mater 321(24):4115–4122. doi:10.1016/J.Jmmm.08.016

van Ommering K, Nieuwenhuis JH, van IJzendoorn LJ, Koopmans B, Prins MWJ (2006) Confined Brownian motion of individual magnetic nanoparticles on a chip: characterization of magnetic susceptibility. Appl Phys Lett 89(14):142511. doi:10.1063/1.2360246

Vojtíšek M, Tarn M, Hirota N, Pamme N (2012) Microfluidic devices in superconducting magnets: on-chip free-flow diamagnetophoresis of polymer particles and bubbles. Microfluid Nanofluidics 13(4):625–635. doi:10.1007/s10404-012-0979-6

Xia YN, Whitesides GM (1998) Soft lithography. Annu Rev Mater Sci 28:153–184. doi:10.1146/Annurev.Matsci.28.1.153

Yellen BB, Hovorka O, Friedman G (2005) Arranging matter by magnetic nanoparticle assemblers. Proc Natl Acad Sci USA 102(25):8860–8864. doi:10.1073/Pnas.0500409102

Zeng J, Chen C, Vedantam P, Brown V, Tzeng TRJ, Xuan XC (2012) Three-dimensional magnetic focusing of particles and cells in ferrofluid flow through a straight microchannel. J Micromech Microeng 22(10):105018. doi:10.1088/0960-1317/22/10/105018

Zhu TT, Marrero F, Mao LD (2010) Continuous separation of non-magnetic particles inside ferrofluids. Microfluid Nanofluidics 9(4–5):1003–1009. doi:10.1007/S10404-010-0616-1

Zhu T, Cheng R, Mao L (2011a) Focusing microparticles in a microfluidic channel with ferrofluids. Microfluid Nanofluidics 11(6):695–701. doi:10.1007/s10404-011-0835-0

Zhu TT, Lichlyter DJ, Haidekker MA, Mao LD (2011b) Analytical model of microfluidic transport of non-magnetic particles in ferrofluids under the influence of a permanent magnet. Microfluid Nanofluidics 10(6):1233–1245. doi:10.1007/S10404-010-0754-5

Zhu TT, Cheng R, Lee SA, Rajaraman E, Eiteman MA, Querec TD, Unger ER, Mao LD (2012) Continuous-flow ferrohydrodynamic sorting of particles and cells in microfluidic devices. Microfluid Nanofluidics 13(4):645–654. doi:10.1007/S10404-012-1004-9